Supporting Information for: Nano-imaging and control of molecular vibrations through electromagnetically induced scattering reaching the strong coupling regime

Eric A. Muller,[*,†] Benjamin Pollard,[†] Hans A. Bechtel,[‡] Ronen Adato,[¶] Dordaneh Etezadi,[§] Hatice Altug,[§] and Markus B. Raschke[*,†]

†*Department of Physics, Department of Chemistry, and JILA, University of Colorado, Boulder, CO, 80309, USA*

‡*Advanced Light Source Division, Lawrence Berkeley National Laboratory, Berkeley, CA 94720*

¶*Departments of Electrical and Computer Engineering and Photonics Center, Boston University, Boston, MA 02215, USA*

§*Institute of Bioengineering, École Polytechnique Fédérale de Lausanne, 1015 Lausanne, Switzerland*

E-mail: eric.muller@colorado.edu; markus.raschke@colorado.edu

19 pages – 7 figures.

Contents

List of Figures **S2**

S1 Methods **S3**

S2 Modeling **S4**

S2.1 Model for Nanowire-Vibration Coupling S5

S2.2 Model for Nanotip-Nanowire Coupling S6

S2.3 Model for Vibrational EIS S7

S3 Pre-Characterization Measurements **S9**

S3.1 Intrinsic Oscillator Response S9

S3.2 Measurement of Nanowire-Vibration Coupling S10

S3.3 Measurement of Nanotip-Nanowire Coupling S11

S4 Effect of Tip Oscillation on Scattering Signal **S13**

S5 Additional Data for Vibrational EIS **S15**

References **S18**

List of Figures

S1 Intrinsic optical response of nanotip, nanowire, and molecular vibrations . . S9

S2 IR absorption and avoided crossing in nanowire-vibration coupling S10

S3 Single wavelength nanoimaging with Si and Au nanotips S11

S4 Spectrally resolved line scan with nanotip-nanowire coupling S12

S5 Effect of Tip Oscillation on Scattering Signal S14

S6 Spectrally resolved line scan with vibrational EIT S16

S7 Anti-crossing in tip-scattered spectra as a function of nanowire resonance . . S16

S8 $Re(\tilde{E}_{scat})$ for dark antenna mode resonance S17

S1 Methods

For s-SNOM measurements, incident light is focused on the imaging tip of an atomic force microscope (AFM). Optical antenna effects within the tip result in evanescent electric fields localized at the tip-sample interface, and large dielectric constants allow metallic AFM tips to act as effective near-field scattering sources throughout the infrared. For both IR *s*-SNOM imaging and spectroscopy, we use metallic Pt/Ir coated AFM tips (Arrow, Nano and More USA) with a 300 kHz resonance frequency and tapping amplitude below 50 nm. IR s-SNOM signal is lock-in demodulated (Zurich Instruments MF2) at the second harmonic of the cantilever frequency. The choice of demodulation frequency represents a trade-off between background suppression, which improves with higher demodulation order, versus the strength of the detected signal, which decreases with increasing demodulation order. Tip-sample approach curves confirm the sensitivity to near-field interactions and sufficient suppression of background scattering, with penetration depth of the near-field signal decaying on a length scale comparable to the tip radius of 20 nm. We observe similar IR *s*-SNOM spectra at the second and third harmonics, albeit at the expense of signal-to-noise.

Tip signal is collected in a back-scattering geometry by the off-axis parabolic mirror with (NA = 0.35) and detected by a liquid nitrogen cooled Mercury Cadmium Telluride detector with 2-11 μm wavelength range (Kollmar Technologies). Interferometric detection in a Michelson geometry also provides optical homodyne amplification of the scattered *s*-SNOM signal as well as suppression of uncontrolled background scattering. In contrast to a symmetric Michelson interferometer, where the sample is placed before or after the interferometer, the AFM tip and sample in are placed at the location of the fixed mirror, enabling phase-resolved detection of the scattered quadrature, $Im(\tilde{E}_{scat})$ and $Re(\tilde{E}_{scat})$, analogous to dispersive Fourier transform spectroscopy. We measure phase-resolved single wavelength

images with a laser based IR *s*-SNOM microscope (Nano-IRs2, Anasys) combined with a tunable quantum cascade laser (QCL, Daylight Solutions) using a pseudoheterodyne detection scheme. Broadband spectroscopy of tip-scattered light is performed using synchrotron illumination (Beamline 5.4, Advanced Light Source) using a modified AFM (Innova, Veeco) combined with a modified FTIR spectrometer (Nicolet 6700, Thermo Fischer).

Spectra were collected at either 8 cm^{-1} or 16 cm^{-1} resolution. Rapid scan spectra were averaged for 1-30 minutes per spectrum. Spectrally resolved transects were measured as a series of 40-60 individual interferograms as the tip is positioned across the nanowire. Far-field IR absorption spectra using far-field Fourier transform infrared (FTIR) spectroscopy using an IR microscope (IFS 66/s, Bruker) with 40x Swarzschild objective. The nanowires are fabricated through a lift-off process using electron beam lithography. PMMA thin films were prepared by spin coating on the nanowires with thickness 8 nm determined by AFM and scanning electron microscopy.

S2 Modeling

We develop a model to predict the optical response of the coupled system consisting of nanowire, nanotip, and molecular vibration, which we treat as harmonic oscillators, with mutual linear coupling terms. The optical transitions of the molecular vibrations, nanowire, and nanotip can be described within the classical limit for low photon flux far from saturation of any transition, which is maintained under the weak illumination conditions in our experiment.[1] The response of the vibrational dipole as well as the electronic response of the nanowire and nanotip can be described by a change in charge displacement x_i, classically described as:

$$\ddot{x}_i + 2\gamma_i \dot{x}_i + \bar{\nu}_0^2 x_i = \frac{1}{2} A \cdot (e^{i\bar{\nu}t} + e^{-i\bar{\nu}t}), \tag{S1}$$

where $\bar{\nu}_0$ is the natural resonance frequency, γ_i is a frictional parameter accounting for dephasing of the molecular or antenna response, $\bar{\nu}$ is the frequency of the driving field, and

A is the amplitude of the driving field.

S2.1 Model for Nanowire-Vibration Coupling

In coupling only two elements, we recover the canonical results including Rabi splitting between resonances of the nanowire and molecular vibration, as well as dispersive Fano line shapes. We treat the electronic displacement for the nanowire x_{wire} and molecular vibration x_{vib}.[1–6] Far-field illumination drives the nanowire with time-dependent oscillating optical field $E_{wire} = \frac{1}{2}A\cdot(e^{i\bar{\nu}t+\phi_{wire}} + e^{-i\bar{\nu}t+\phi_{wire}})$ directly, while excitation of the molecular vibration is assumed to be induced through near-field energy transfer only. We can write the equations of motion as:

$$\ddot{x}_{wire} + \bar{\nu}_{wire}^2 x_{wire} + 2\gamma_{wire}\dot{x}_{wire} - k_{wire,vib}(x_{wire} - x_{vib}) = \frac{e}{m}\tilde{E}_{wire}(t), \tag{S2a}$$

$$\ddot{x}_{vib} + \bar{\nu}_{vib}^2 x_{vib} + 2\gamma_{vib}\dot{x}_{vib} - k_{wire,vib}(x_{vib} - x_{wire}) = 0, \tag{S2b}$$

with resonance frequencies $\bar{\nu}_{wire}$, and $\bar{\nu}_{vib}$ and corresponding damping rates γ_{wire}, and γ_{vib}. Near-field coupling between the nanowire and molecular vibration is included as the coupling strength $\bar{\nu}_{wire,vib}$, which can be related to the spring constant k in the familiar mass and spring models through the equation $\bar{\nu} = \sqrt{k/m}$.

We seek plane wave solutions of the form $x_i = A_i\cdot e^{i\bar{\nu}t}$, resulting in:

$$(\bar{\nu}^2 - \bar{\nu}_{wire}^2 + 2i\gamma_{wire}\bar{\nu})x_{wire} - k_{wire,vib}(x_{wire} - x_{vib}) = \frac{e}{m}\tilde{E}_{wire}(\bar{\nu}), \tag{S3a}$$

$$(\bar{\nu}^2 - \bar{\nu}_{vib}^2 + 2i\gamma_{vib}\bar{\nu})x_{vib} - k_{wire,vib}(x_{wire} - x_{vib}) = 0. \tag{S3b}$$

We then rewrite this system of equations as:

$$\begin{bmatrix} g_{wire} & k_{wire,vib} \\ k_{wire,vib} & g_{vib} \end{bmatrix} \cdot \begin{bmatrix} x_{wire} \\ x_{vib} \end{bmatrix} = \begin{bmatrix} \tilde{E}_{wire} \\ 0 \end{bmatrix}, \tag{S4}$$

where we have substituted $g_{wire} = \bar{\nu}^2 - \bar{\nu}_{wire}^2 + 2i\gamma_{wire}\bar{\nu} - k_{wire,vib}$ and $g_{vib} = \bar{\nu}^2 - \bar{\nu}_{vib}^2 + 2i\gamma_{vib}\bar{\nu} - k_{wire,vib}$.

Solving for the eigenfrequencies, we find the adiabatic resonance frequencies of the hybridized modes $\bar{\nu}_\pm$ in the case of small damping

$$\bar{\nu}_\pm^2 = \frac{1}{2}\left[\bar{\nu}_{wire}^2 + \bar{\nu}_{vib}^2 + 2k_{wire,vib} \pm \sqrt{(\bar{\nu}_{wire}^2 - \bar{\nu}_{vib}^2)^2 + 4\bar{\nu}_{wire,vib}^4}\right]. \tag{S5}$$

Thus, with increasing $\bar{\nu}_{wire,vib}$, this hybridized mode forms two branches $\bar{\nu}_\pm$, with a gap proportional to the coupling strength. We then solve for the steady state solutions of the resulting polarization of the wire and vibration.

$$P_{wire} = e \cdot \frac{\tilde{E}_{wire} \cdot g_{vib}}{g_{wire} \cdot g_{vib} - k_{wire,vib}^2}, \tag{S6a}$$

$$P_{vib} = e \cdot \frac{\tilde{E}_{wire} \cdot k_{wire,vib}}{k_{wire,vib}^2 - g_{wire} \cdot g_{vib}}, \tag{S6b}$$

where the polarization of the nanowire P_{wire} and the vibration P_{vib} are both dependent on the resonant response of each element and associated near-field coupling. In the detected FTIR absorption of the nanowire array, only the nanowire couples to the far-field and the scattered light from the nanowire is proportional to P_{wire}.

S2.2 Model for Nanotip-Nanowire Coupling

We next model the case of coupling between the nanowire and nanotip. Far-field illumination drives the nanotip with time-dependent oscillating optical field $E_{tip} = A \cdot e^{i\bar{\nu}t + \phi_{tip}}$. The nanowire similarly is driven by the optical field $E_{wire} = A \cdot e^{i\bar{\nu}t + \phi_{wire}}$, with the phase retardation between nanotip and nanowire $\Delta\Phi = \phi_{tip} - \phi_{wire}$. Equations S2a and S2b then take

the form:

$$\ddot{x}_{wire} + \bar{\nu}_{wire}^2 x_{wire} + 2\gamma_{wire}\dot{x}_{wire} - k_{tip,wire}(x_{wire} - x_{tip}) = \frac{e}{m}\tilde{E}_{wire}(t), \text{and} \tag{S7a}$$

$$\ddot{x}_{tip} + \bar{\nu}_{tip}^2 x_{tip} + 2\gamma_{tip}\dot{x}_{tip} - k_{tip,wire}(x_{tip} - x_{wire}) = \frac{e}{m}\tilde{E}_{tip}(t). \tag{S7b}$$

These equations of motion represent a generalization of previous models,[1,2,5,6] as we include the optical driving field for both resonators.

We seek the plane wave solutions of these coupled equations of motion as before. Using:

$$\begin{bmatrix} g_{tip} & k_{tip,wire} \\ k_{tip,wire} & g_{wire} \end{bmatrix} \cdot \begin{bmatrix} x_{wire} \\ x_{vib} \end{bmatrix} = \begin{bmatrix} \tilde{E}_{tip} \\ \tilde{E}_{wire} \end{bmatrix}, \tag{S8}$$

with $g_{tip} = \bar{\nu}^2 - \bar{\nu}_{tip}^2 + 2i\gamma_{tip}\bar{\nu} - k_{tip,wire}$ and $g_{wire} = \bar{\nu}^2 - \bar{\nu}_{wire}^2 + 2i\gamma_{wire}\bar{\nu} - k_{tip,wire}$, we obtain:

$$P_{tip} = e \cdot \frac{\tilde{E}_{tip} \cdot g_{wire} + \tilde{E}_{wire} \cdot k_{tip,wire}}{g_{tip} \cdot g_{wire} - k_{tip,wire}^2} \tag{S9}$$

where the driving fields of the nanotip and nanowire include the phase delay due to the geometric path difference as stated above. We can then calculate the tip-scattered optical field $\tilde{E}_{tip} \propto P_{tip}$, as a function of incident illumination and near-field coupling between the nanowire and nanotip.

S2.3 Model for Vibrational EIS

We next model the case of coupling between the nanowire and nanotip and molecular vibration. We include driving of the nanotip and nanowire as before. We introduce near-field coupling between the nanowire and molecular vibrations $\bar{\nu}_{wire,vib}$, between the nanotip and nanowire $\bar{\nu}_{tip,wire}$ and between the nanotip and molecular vibrations $\bar{\nu}_{tip,vib}$ as an extension

of the models above, leading to:

$$\ddot{x}_{tip} + 2\gamma_{tip}\dot{x}_{tip} + \bar{\nu}_{tip}^2 x_{tip} - k_{tip,wire}(x_{tip} - x_{wire}) - k_{tip,vib}(x_{tip} - x_{vib}) = \frac{e}{m}\tilde{E}_{tip}(t), \tag{S10a}$$

$$\ddot{x}_{wire} + 2\gamma_{tip}\dot{x}_{wire} + \bar{\nu}_{wire}^2 x_{wire} - k_{tip,wire}(x_{wire}x_{tip}) - \bar{\nu}_{wire,vib}^2(x_{wire} - x_{vib}) = \frac{e}{m}\tilde{E}_{wire}(t), \tag{S10b}$$

$$\ddot{x}_{vib} + 2\gamma_{vib}\dot{x}_{vib} + \bar{\nu}_{vib}^2 x_{vib} - \bar{\nu}_{wire,vib}^2(x_{vib} - x_{wire}) - k_{tip,vib}(x_{vib} - x_{tip}) = 0, \tag{S10c}$$

with resonance frequencies $\bar{\nu}_{tip}$, $\bar{\nu}_{wire}$, and $\bar{\nu}_{vib}$ and corresponding damping rates γ_{tip}, γ_{wire}, and γ_{vib}. Assuming plane wave solutions, we can express the system of equations as:

$$\begin{bmatrix} g_{tip} & k_{tip,wire} & k_{tip,vib} \\ k_{tip,wire} & g_{wire} & k_{wire,vib} \\ k_{tip,vib} & k_{wire,vib} & g_{vib} \end{bmatrix} \cdot \begin{bmatrix} x_{tip} \\ x_{wire} \\ x_{vib} \end{bmatrix} = \begin{bmatrix} \tilde{E}_{tip} \\ \tilde{E}_{wire} \\ 0 \end{bmatrix}. \tag{S11}$$

In the absence of coupling, the frequency dependent electronic displacement for each oscillator (x_{tip}, x_{wire}, and x_{vib}) takes the form of a Lorentzian response, which appear along the diagonal as $g_{wire} = \bar{\nu}^2 - \bar{\nu}_{wire}^2 + 2i\gamma_{wire}\bar{\nu} - k_{tip,wire} - k_{vib,tip}$, $g_{tip} = \bar{\nu}^2 - \bar{\nu}_{tip}^2 + 2i\gamma_{tip}\bar{\nu} - k_{tip,wire} - \bar{\nu}_{vib,wire}^2$, and $g_{vib} = \bar{\nu}^2 - \bar{\nu}_{vib}^2 + 2i\gamma_{vib}\bar{\nu} - k_{tip,vib} - k_{wire,vib}$. With the addition of near-field coupling, energy transfer between the oscillators occurs with rates $\bar{\nu}_{tip,wire}$, $\bar{\nu}_{wire,vib}$, and $\bar{\nu}_{tip,vib}$. The polarization of the nanotip becomes:

$$P_{tip} = e \cdot \frac{(\tilde{E}_{tip}(g_{wire}g_{vib} + \bar{\nu}_{wire,vib}^4) - \tilde{E}_{wire}(g_{vib}k_{tip,wire} - k_{tip,vib}k_{wire,vib})}{g_{tip}(g_{wire}g_{vib} - \bar{\nu}_{wire,vib}^4) - g_{vib}\bar{\nu}_{tip,wire}^4 - g_{wire}k_{tip,vib}^2 + 2k_{tip,wire}k_{tip,vib}k_{wire,vib}}. \tag{S12}$$

In the experiment, we selectively detect the tip scattered optical field $\tilde{E}_{tip} \propto P_{tip}$. In the main text we simplify this equation for the case of $\bar{\nu}_{tip,vib} = 0$ in Eq. 1 with units of wavenumbers $\bar{\nu} = \sqrt{\frac{k}{m}}$, and we include the full equation accounting for $\bar{\nu}_{tip,vib}$ in Eq. 2. From these two

equations, we predict the spectroscopic signatures of induced tip polarization as a function of coupling between tip, wire, and molecular vibration, and accounting for its optical excitation through nanotip or nanowire.

S3 Pre-Characterization Measurements

S3.1 Intrinsic Oscillator Response

We first measure the intrinsic optical response of each of the three oscillators.The Pt/Ir nanotip is illuminated with broadband (700-5000 cm^{-1}) synchrotron radiation while operating in intermittent contact mode (cantilever frequency ~250 kHz) above a non-resonant gold sample. Figure S1A shows the resulting spectrum measured interferometrically at the second demodulation frequency of the cantilever normalized to the spectrum of the synchrotron measured by the same interferometer. The slowly varying optical response over this large spectral range confirms the broadband response of the nanotip.

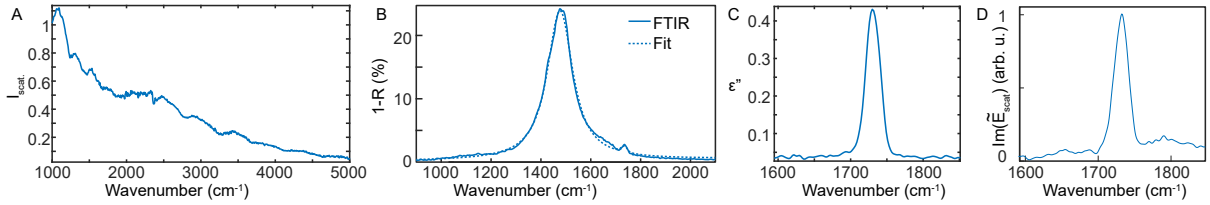

Figure S1: (A) SINS measured from the bare nanotip above a bare Au substrate showing the non-resonant response of the tip. (B) FTIR absorption spectrum of a nanowire array using a far-field IR microscope. Dotted line indicates Lorentzian fit to the nanowire resonance at 1480 cm^{-1} and the weakly enhanced response of the PMMA at 1730 cm^{-1} (C) Dielectric permittivity ϵ'' of poly(methyl methacrylate) as measured by IR spectroscopic ellipsometry showing the carbonyl stretch region. (D) Tip-scattered SINS spectrum from a 20 nm thickness of PMMA on a non-resonant substrate.

Figure S1B shows the spectrum from an array of nanowires measured by an FTIR microscope, from which we determine $\bar{\nu}_{wire}$ and γ_{wire}. Fig. S1C shows the narrow response of the carbonyl vibration from a thick film of PMMA as measured by infrared spectroscopic ellipsometry, expressed as ϵ" with line width of 21 ± 2 cm^{-1}. Figure S1D shows the SINS

spectrum of PMMA spin coated as a 20 nm thin film on a flat Au substrate, with an optical response in agreement with that measured by spectroscopic ellispometry. The nanotip increases sensitivity to PMMA significantly in comparison to far-field methods, which were unable to detect PMMA for the film thicknesses used in the antenna experiment.

S3.2 Measurement of Nanowire-Vibration Coupling

In order to quantify the near-field coupling strength between the nanowire and molecular vibration, we vary the nanowire resonance across the carbonyl stretching mode of PMMA at 1730 cm^{-1} as indicated in Fig. S2A. Far-field FTIR absorption (Fig. S2B, solid lines) of PMMA coated nanowires shows the emergence of an enhanced vibrational response. The vibrational mode appears as a small peak when the resonance frequency $\bar{\nu}_{wire}$ is far from $\bar{\nu}_{vib}$, increasing as the nanowire is tuned near to degeneracy with the carbonyl resonance.

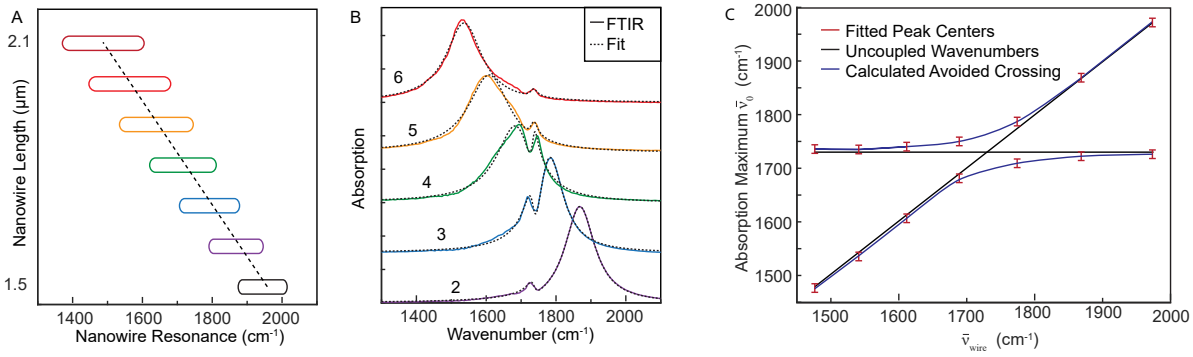

Figure S2: (A) Schematic showing set of nanowires with varying lengths and corresponding antenna resonance $\bar{\nu}_{wire}$. (B) Absorption spectra of nanowires with varying lengths coupled to molecular vibrations (solid) with fits to two oscillator model (dotted). (C) Center frequencies of the upper and lower branches ($\bar{\nu}_{\pm}$) as determined by fits to FTIR absorption from PMMA coated nanowires. The avoided crossing (adiabatic, red) is compared with the resonance of the bare nanowire and wavenumber of the carbonyl vibrational mode (black, diabatic).

As the resonant frequency of the nanowire approaches that of the molecular vibration, we observe Rabi splitting of the two modes. We then fit the measured peak centers to an avoided crossing as given by Eq. S5 with the measured parameters for the uncoupled nanowires and molecular vibrations $\bar{\nu}_{wire}$, $\bar{\nu}_{vib}$, γ_{wire}, and γ_{vib} as constant. Fits to the FTIR

reflectance spectra (Fig. S2B calculated using Eq. S6a with $\bar{\nu}_{wire,vib} = 47 \pm 5\,\mathrm{cm}^{-1}$ shows close agreement betweend calculated and experimentally measured line shapes. From the fits, we determine the coupling strength to be $\bar{\nu}_{wire,vib} = 47 \pm 5\,\mathrm{cm}^{-1}$. The measured adiabatic energy levels (Fig. S2C, red) and associated coupling strength closely agrees with fits from Eq. S5, demonstrating Rabi splitting when compared to (Fig. S2C, black) the diabatic energy levels the uncoupled oscillators.

S3.3 Measurement of Nanotip-Nanowire Coupling

We measure the scattering of the coupled nanotip and nanowire by single-frequency s-SNOM. By positioning nanotips of different materials above the nanowire and thin film polymer, we can modify the coupling between the nanotip and nanowire. Fig. 2A,B of the main text show the tip scattered $Im(\tilde{E}_{scat})$ and $Re(\tilde{E}_{scat})$ signal measured near the antenna resonance at 1775 cm^{-1} using vertically polarized light and a Pt coated tip, revealing an anti-symmetric image. In contrast, in Figure S3A-C, we show the tip scattered $Im(\tilde{E}_{scat})$ and $Re(\tilde{E}_{scat})$ images measured with a Si nanotip. We further reduce far-field driving of the nanotip response by illuminating with linearly polarized light oriented so that the electric field component of the light is near-parallel with the nanowire transition dipole yet is perpendicular to the more polarizable long axis of the nanotip. We observe a symmetric pattern in the $Im(\tilde{E}_{scat})$ and $Re(\tilde{E}_{scat})$ images due to the reduced coupling and far-field excitation of the nanotip.

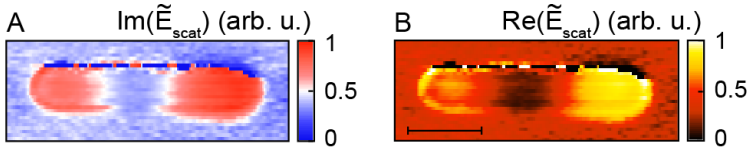

Figure S3: Image of tip scattered (A) $Im(\tilde{E}_{scat})$ and (B) $Re(\tilde{E}_{scat})$ measured with Si nanotip with laser tuned to 1775 cm^{-1} Scale bars 500 nm.

Symmetric near-field images of nanowire field distribution as seen in Fig. S3A,B have been previously attributed to weak coupling between nanotip and nanowire.[7] The emergence of anti-symmetric images (Fig. 2A,B of main text) when using a metallic nanotip have been

attributed to strong coupling between nanotip and nanowire.[8,9] Our results agree with the previously empirically observed near-field images using metal nanotips, although as with previous investigations, quantification of the coupling strength is not possible through single wavelength imaging.

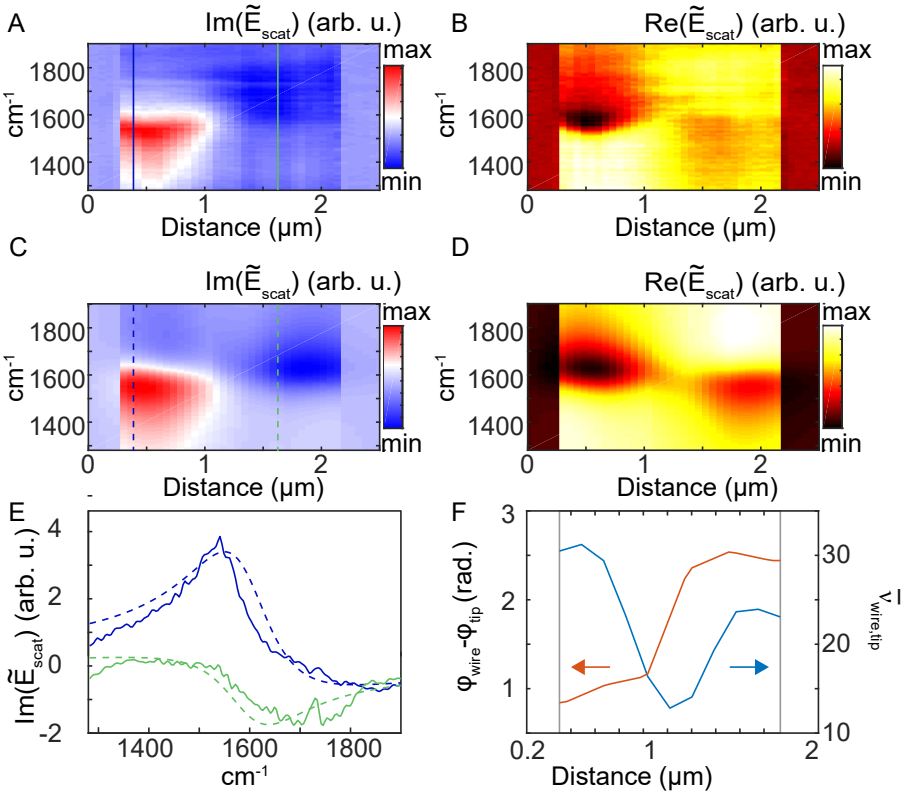

Figure S4: (A-B) Spatio-spectral line scan of $Im(\tilde{E}_{scat})$ and $Re(\tilde{E}_{scat})$ with (C-D) corresponding fit along the length of a nanowire with antenna resonance frequency $\bar{\nu}_{wire} = 1610\,\mathrm{cm}^{-1}$, selected to be away from PMMA vibrational resonances. (E) $Im(\tilde{E}_{scat})$ spectra (solid) and model fits (dashed) with tip positioned near left (blue) and right (green) terminals of the antenna as indicated in (A and C). (F). Fitted model parameters $\Delta\Phi$ and $\bar{\nu}_{tip,wire}$ for calculated spectra (C-D).

We next measure nanotip-nanowire coupling through broadband spectroscopy of nanotip scattering. Figure S4A-B present surface plots representing a spatio-spectral line scan of $Im(\tilde{E}_{scat})$ and $Re(\tilde{E}_{scat})$ measured along the long axis of the nanowire. $Im(\tilde{E}_{scat})$ is positive with an absorptive line shape on the left terminal and is negative on the right terminal. Similarly, $Re(\tilde{E}_{scat})$ has normal versus anomalous dispersion on the left and right terminals, respectively. We fit the experimentally measured spectra using Eq. S12 in order to determine

coupling rates. For each fit, we use the previously determined uncoupled optical response of the nanotip and nanowire and as fixed parameters from above with non-resonant nanotip, $\bar{\nu}_{wire} = 1640\,\mathrm{cm}^{-1}$ and $\Gamma_{wire} = 100\,\mathrm{cm}^{-1}$, while varying the position-dependent near-field coupling $\bar{\nu}_{tip,wire}$ and phase retardation $\Delta\Phi$. Calculated spectra shown as a surface plot in Fig. S4C-D reproduce the observed sign inversion of $Im(\tilde{E}_{scat})$ and $Re(\tilde{E}_{scat})$ as a function of tip position. Figure S4E (solid lines) shows corresponding individual spectra and fits with positive absorptive line shape near the left terminal (blue), with sign reversal near the right terminal (green). From the fits in Fig. S4C-D, we find that $\Delta\Phi$ increases by $\pi/2$ radians across the length of the nanowire, shown in Fig. S4F. We also measure $\bar{\nu}_{tip,wire}$ and find its value is found to vary from 12-32 cm^{-1}. The coupling $\bar{\nu}_{tip,wire}$ is small with the nanotip near the center of the nanowire, and greatest with the nanotip near the terminals.

S4 Effect of Tip Oscillation on Scattering Signal

We detect the scattered signal at the second-harmonic of the AFM tip oscillation, operating the tip with a 50 nm tapping amplitude. As established in s-SNOM the detection at second- and higher harmonics of the cantilever motion allows for near-field signal discrimination against the far-field background.[10] The associated distance dependent coupling does modify the line shape of the near-field scattering spectrum in general.[11,12] However, for uncoupled molecular vibrations including coupling of molecular vibrations to the nanowire, the spectral variations, also as a function of detected harmonics, is minimal, and does not modify or overwhelm the observed plasmonic analogues of EIT/EIA spectral features. This can be seen in Fig. S5A where we model the spectral response for different detection harmonics. We consider a tip oscillating sinusoidally above the nanowire with a 50 nm peak-to-peak amplitude (blue) as a function of time. For a distance dependent coupling $1/z^4$ to first order, as expected for a dipole-dipole interaction[13] (and references therein), we calculate the coupling between the nanotip and nanowire near the optical resonance frequency of the

nanowire. We show the tip-sample coupling as a function of tip-sample distance in the time domain of the oscillating tip (red dotted in Fig. S5A).

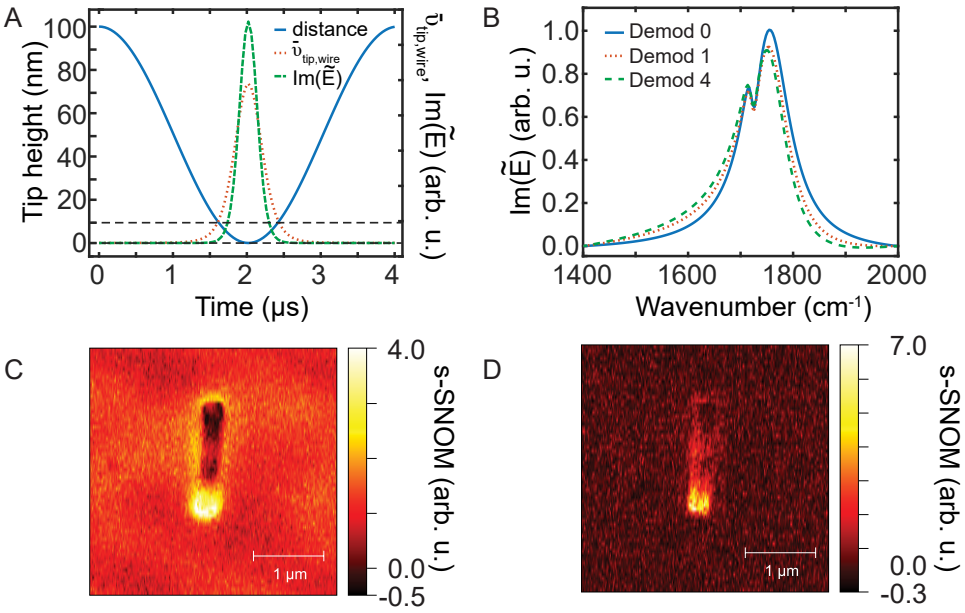

Figure S5: (A) Calculation as a function of tip-sample distance (blue) of tip-wire coupling (red dotted) and tip scattered signal near the nanowire resonance (green dashed). (B) Calculation of tip scattered spectra for (blue) stationary tip as well as with a tip operating in tapping mode with lock in detection (red dotted) at the first harmonic of the tip oscillation frequency, and (green dashed) at the fourth harmonic of the tip oscillation frequency, showing minimal different and no adverse effect on the EIT dip. (C) Image of scattered light with using SINS detected at first harmonic of the tip oscillation, and (D) fourth harmonic of the tip oscillation, exhibiting no discernible difference in spatial distribution of phase dependent coupling.

Adding the distance-dependent nanotip-nanowire coupling to equation S12 from above, we can calculate the induced polarization of the oscillating nanotip (green dashed), corresponding to the scattered near-field signal. Figure S5B shows the resulting tip scattered spectra normalized for clarity as calculated first for a hypothetically stationary tip in continuous tip-sample interaction at the sample surface (blue), in comparison to the spectra simulating the lock-in demodulation at different harmonics (for better clarity, showing the lowest first harmonic (red dotted) and highest fourth harmonic (green dashed) of the tip oscillation only). Comparing the four demodulated and non-demodulated spectra, there is a only small spectral shift and lineshape variation that does not interfere or adversely affect the

observation of the EIT/EIA-like spectral feature as seen in the normalized spectra. Further extension of these calculations to model also extremely small tip oscillations suggests that the distance dependent coupling of the nanotip to molecular vibration and nanowire and resulting interference of excitation pathways could affect the observed spectra for tapping amplitudes below 10 nm. For the tapping amplitude of 50 nm used in these experiments, however, the demodulation primarily increases sensitivity and reduces background signal. Figure S5C-D shows for synchrotron *s*-SNOM signal detected at the (S5C) the first harmonic with large signal levels and a visible far-field background seen as slowly varying signal across the image, compared with (S5D) the fourth harmonic of the tip oscillation with reduced far-field background at the expense of overall lower signal quality.

S5 Additional Data for Vibrational EIS

We quantify near-field coupling through broadband IR *s*-SNOM spectroscopy measured as a function of tip position. Figure 2B of the main text is reproduced in Fig. S6A, presenting a surface plot of $Im(\tilde{E}_{scat})$ spectra from a transect (dotted line in (A)) across the nanowire. The spectrum of $Im(\tilde{E}_{scat})$ has primarily absorptive character near the left antenna terminal with sign reversal near the right antenna terminal. Figure S6B shows the corresponding simultaneously detected $Re(\tilde{E}_{scat})$ from the line scan as a surface plot. $Re(\tilde{E}_{scat})$ exhibits normal versus anomalous dispersion on the left and right terminals, respectively. The vibrational response at 1730 cm^{-1} is observed prominently on the left terminal of both the $Re(\tilde{E}_{scat})$ and $Im(\tilde{E}_{scat})$ line scans.

From fitting the spectra using Eq. S12 we quantify the near-field coupling. As discussed in the main text, the position-dependent coupling strength traces the calculated sinusoidal current distribution for the dipole resonance of a half wavelength nanowire (dashed).[7] We show in Fig. S6C-D a surface plot of calculated fits for $Im(\tilde{E}_{scat})$ for each of the 42 spectra of the line scan. Spectra are calculated in the complex plane and simultaneously fit to both

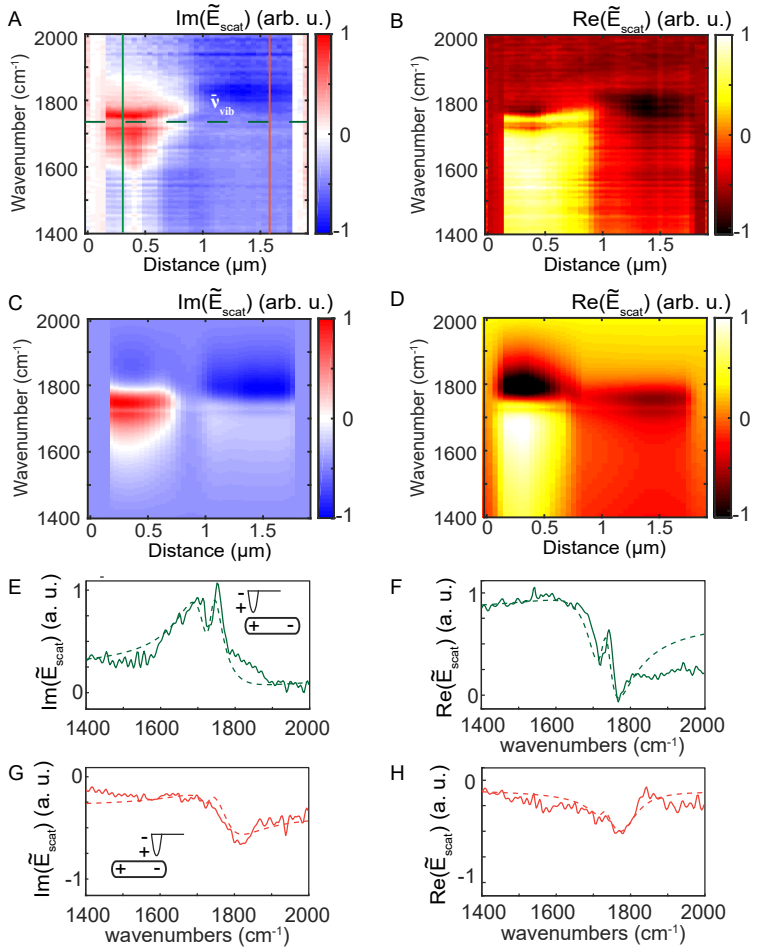

Figure S6: Spatio-spectral line scan of (A) $Im(\tilde{E}_{scat})$ and (B) $Re(\tilde{E}_{scat})$ measured along the length of the nanowire with (C-D) corresponding fit. (E) $Im(\tilde{E}_{scat})$ and (F) $Re(\tilde{E}_{scat})$ spectra (solid) and model fits (dashed) measured on the left terminal. (G-H) Corresponding tip scattered spectra and fit (solid and dashed, respectively) measured at the right terminal.

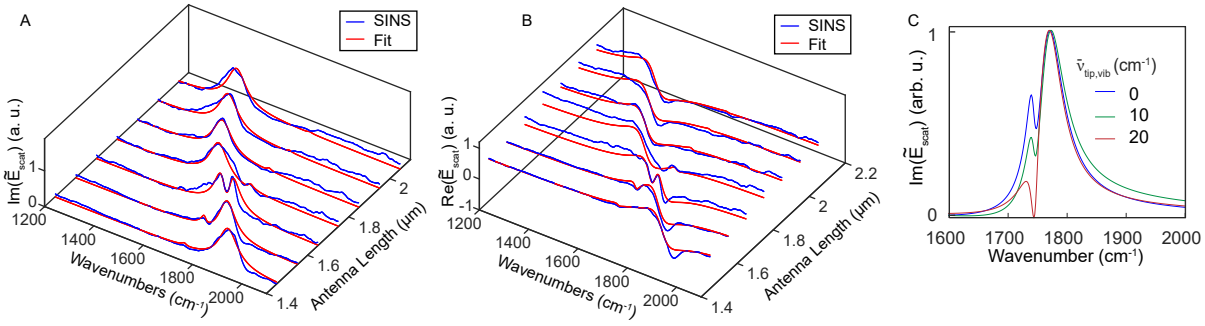

Figure S7: Tip scattered quadrature (A) $Im(\tilde{E}_{scat})$ and (B) $Re(\tilde{E}_{scat})$ (blue) with corresponding complex valued fits (red) measured for a set of different nanowire lengths. (C) Calculated $Im(\tilde{E}_{scat})$ as a function of $\bar{\nu}_{tip,vib}$.

$Re(\tilde{E}_{scat})$ and $Im(\tilde{E}_{scat})$. Finally, we show in Fig. S6E-H the full quadrature of the measured and calculated $Re(\tilde{E}_{scat})$ and $Im(\tilde{E}_{scat})$ on each terminal of the nanowire, for which only $Im(\tilde{E}_{scat})$ is shown in Fig. 2B of the main text.

We measure $Im(\tilde{E}_{scat})$ as a function of nanowire length Fig. S7C. The nanotip is positioned 100 nm from the left terminal of the nanowire in order to minimize phase retardation between nanowire and nanotip leading. Fig. 2G of the main text shows $Im(\tilde{E}_{scat})$ for a set of 5 nanowire lengths. Figure S7A-B show a larger data set of tip scattered spectra collected across 7 nanowire lengths, including both $Im(\tilde{E}_{scat})$ and $Re(\tilde{E}_{scat})$ (blue with corresponding calculated spectra (red), which we fit simultaneously in the complex plane.

We next estimate vibrational excitation through the nanotip $\bar{\nu}_{tip,vib}$ when coupled to the bright mode of the nanowire. Figure S7C shows calculated $Re(\tilde{E}_{scat})$ as a function of $\bar{\nu}_{tip,vib}$ with constant $\bar{\nu}_{wire,vib}$. Varying the fit parameter $\bar{\nu}_{tip,vib}$ over the range $0 \leq \bar{\nu}_{tip,vib} \leq 10$ cm^{-1} only small changes are observed in the spectra (blue and green). Only for larger values of $\bar{\nu}_{tip,vib} = 20$ cm^{-1} (red), interference with nanotip excitation leads to an increased spectral dip at the vibrational resonance. Comparing with experimentally measured spectra, we estimate an upper bound for $\bar{\nu}_{tip,vib}$ of 15 cm^{-1}. We therefore attribute the spectral dip to electromagnetically induced transparency (EIT) and coupling $\bar{\nu}_{wire,vib}$ with negligible contribution from $\bar{\nu}_{tip,vib}$.

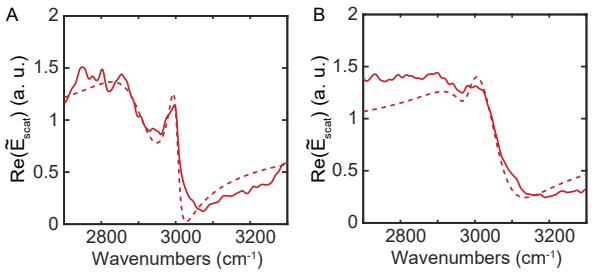

Figure S8: (A-B) Tip scattered $Re(\tilde{E}_{scat})$ measured as a transect along the nanowire, with corresponding surface plot of $Im(\tilde{E}_{scat})$ shown in Fig. 2 of the main text. (C-D) $Re(\tilde{E}_{scat})$ with $\bar{\nu}_{wire} = 2960$ cm^{-1} and (D) $\bar{\nu}_{wire} = 3200$ cm^{-1} with corresponding calculated fits (dashed). Corresponding $Im(\tilde{E}_{scat})$ shown in Fig. 3 C-D of the main text.

Finally, Fig. S8A-B show the measured $Re(\tilde{E}_{scat})$ spectra and corresponding fits for the

plasmonic analogues of EIS, for which only $Im(\tilde{E}_{scat})$ was discussed in the main text. Figures 3C and 3E of the main text show the associated $Im(\tilde{E}_{scat})$ spectra and calculated fits.

References

(1) Souza, J. A.; Cabral, L.; Oliveira, R. R.; Villas-Boas, C. J. Electromagnetically-induced-transparency-related phenomena and their mechanical analogs. *Phys. Rev. A* **2015**, *92*, 023818.

(2) Joe, Y. S.; Satanin, A. M.; Kim, C. S. Classical analogy of Fano resonances. *Phys. Scr.* **2006**, *74*, 259–266.

(3) Zhang, S.; Genov, D. A.; Wang, Y.; Liu, M.; Zhang, X. Plasmon-Induced Transparency in Metamaterials. *Phys. Rev. Lett.* **2008**, *101*, 047401.

(4) Wu, X.; Gray, S. K.; Pelton, M. Quantum-dot-induced transparency in a nanoscale plasmonic resonator. *Opt. Express* **2010**, *18*, 23633–23645.

(5) Novotny, L. Strong coupling, energy splitting, and level crossings: A classical perspective. *Am. J. Phys.* **2010**, *78*, 1199–1202.

(6) Taubert, R.; Hentschel, M.; Kästel, J.; Giessen, H. Classical Analog of Electromagnetically Induced Absorption in Plasmonics. *Nano Lett.* **2012**, *12*, 1367–1371.

(7) Olmon, R. L.; Rang, M.; Krenz, P. M.; Lail, B. A.; Saraf, L. V.; Boreman, G. D.; Raschke, M. B. Determination of Electric-Field, Magnetic-Field, and Electric-Current Distributions of Infrared Optical Antennas: A Near-Field Optical Vector Network Analyzer. *Phys. Rev. Lett.* **2010**, *105*, 167403.

(8) García-Etxarri, A.; Romero, I.; García de Abajo, F. J.; Hillenbrand, R.; Aizpurua, J. Influence of the tip in near-field imaging of nanoparticle plasmonic modes: Weak and strong coupling regimes. *Phys. Rev. B* **2009**, *79*, 125439.

(9) Habteyes, T. G. Direct Near-Field Observation of Orientation-Dependent Optical Response of Gold Nanorods. *J. Phys. Chem. C* **2014**, *118*, 9119–9127.

(10) Ocelic, N.; Huber, A.; Hillenbrand, R. Pseudoheterodyne detection for background-free near-field spectroscopy. *Appl. Phys. Lett.* **2006**, *89*, 101124.

(11) Amarie, S.; Keilmann, F. Broadband-infrared assessment of phonon resonance in scattering-type near-field microscopy. *Phys. Rev. B* **2011**, *83*, 045404.

(12) Wang, L.; Xu, X. G. Scattering-type scanning near-field optical microscopy with reconstruction of vertical interaction. *Nat. Commun.* **2015**, *6*, 8973.

(13) Atkin, J. M.; Berweger, S.; Jones, A. C.; Raschke, M. B. Nano-optical imaging and spectroscopy of order, phases, and domains in complex solids. *Adv. Phys.* **2012**, *61*, 745–842.